International Journal of Technology 10(1): 200-211
ISSN 2086-9614

CASCADE OPTIMIZATION OF AN AXIAL-FLOW HYDRAULIC TURBINE TYPE PROPELLER BY A GENETIC ALGORITHM

Qidun Maulana Binu Soesanto[1*], Puji Widiyanto[1], Anjar Susatyo[1], Edwar Yazid[1]

[1]*Research Centre for Electrical Power and Mechatronics (P2 Telimek), Indonesian Institute of Sciences (LIPI), Komplek LIPI, Jl. Cisitu No. 21/154D, Bandung 40135, Indonesia*

(Received: March 2018 / Revised: April 2018 / Accepted: October 2018)

ABSTRACT

This study proposes the use of the genetic algorithm (GA) method in hydraulic turbine optimization for renewable energy applications. The algorithm is used to optimize the performance of a two-dimensional hydrofoil cascade for an axial-flow hydraulic turbine. The potential flow around the cascade is analyzed using the surface vorticity panel method, with a modified coupling coefficient to deal with the turbine cascade. Each section of the guide vane and runner blade hydrofoil cascade is optimized to satisfy the shock-free criterion, which is the fluid dynamic ideal to achieve minimum profile losses. Comparison is also made between the direct and random switching methods for the GA crossover operator. The optimization results show that the random switching method outperforms the performance of the direct switching method in terms of the resulting solutions, as well as in terms of the computational time required to reach convergence. As an alternative to experimental trials, the performance of both turbine designs are predicted and analyzed using the three-dimensional computational fluid dynamics (CFD) approach under several operating conditions. The simulation results show that the optimized design, which is obtained by applying the shock-free criterion using the GA, successfully improves the performance of the initial turbine design.

Keywords: Axial-flow hydraulic turbine; Computational fluid dynamics; Genetic algorithm; Shock-free criterion

1. INTRODUCTION

Hydrodynamic performance analysis is important for optimizing the hydraulic performance of axial-flow hydraulic turbines. The common method is by analyzing the fluid-dynamic behavior around the hydrofoil using a two-dimensional cascade, which is an infinite array of hydrofoils on a two-dimensional (x,y) plane. Several research studies have been conducted to optimize axial-flow hydraulic performance by minimizing hydrofoil losses using certain criteria, such as the minimum suction pressure coefficient (da Cruz et al., 2008; Sutikno & Adam, 2011) and the shock-free inflow criterion, as in the work of Muis et al. (2015, 2016). In addition, the performance of the optimized design needs to be predicted based on real conditions, before prototyping takes place. The three-dimensional computational fluid dynamics (CFD) approach based on the finite volume method is an efficient fluid dynamic tool to predict the performance of turbomachinery, such as hydraulic turbines. This approach allows the prediction of certain flow parameters in complex flow phenomena, which are difficult to obtain experimentally, such as the velocity and pressure contours at any location in the computational domain.

*Corresponding author's email: qidu002@lipi.go.id, Tel. +62-22-2503055, Fax. +62-22-2504773
Permalink/DOI: https://doi.org/10.14716/ijtech.v10i1.1744

This research aims to optimize the performance of an axial-flow hydraulic turbine using the genetic algorithm (GA) method, which is an evolutionary optimization algorithm based on natural selection. The algorithm is used to find the optimal design variables to achieve the shock-free criterion (Lewis, 1996).

During the optimization process, the potential flow around the two-dimensional cascade is analyzed using the surface vorticity panel method (Lewis, 1991). The performance of the initial and optimized turbine designs is predicted using the three-dimensional CFD approach, which has previously been used by several researchers (Drtina & Sallaberger, 1999; Prasad, 2012; Ramos et al., 2013; Schleicher et al., 2015; Riglin et al., 2016; Kim et al., 2017; Kinsey & Dumas, 2017) to predict the performance and flow behavior of hydraulic turbines. Subsequently, the performance of both turbine designs is compared and analyzed.

2. METHODS

2.1. Turbine Design

The basic shape of the guide vane and runner blade was designed using a four-digit NACA airfoil. A comprehensive explanation of the airfoil was presented by Jacobs et al. (1933). In this study, each guide vane and runner blade geometry is divided into five equal sections, from hub (1) to tip (5), as shown in Figures 1a and 1b.

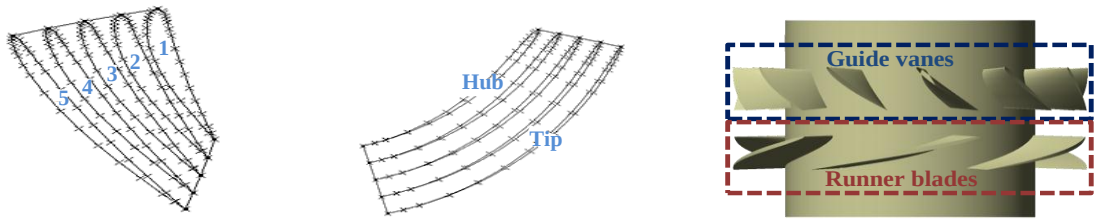

(a) (b) (c)

Figure 1 Each hydrofoil section of the axial-flow hydraulic turbine

As a result, the initial design of the axial-flow hydraulic turbine is as shown in Figure 1c. In this study, the turbine geometry was designed as a scaled-down model of a geometrically similar prototype. The chosen model geometry and its operating conditions, which comprise a net head for very low head sites, volumetric flow rates, and a dimensionless specific speed, have been adjusted so that the model can be characterized in a laboratory-scale environment. The equation for the specific speed, N_s, refers to the international standard for model acceptance tests of hydraulic turbines, storage pumps and pump-turbines, IEC 60193 (International Electrotechnical Commission, 1999). Referring to the type of turbine as a function of its specific speed, the current model matches the propeller or kaplan turbine type (Bostan et al., 2013). In this study, an axial-flow hydraulic turbine type propeller with fixed guide vanes and runner blades was chosen because it displays good performance when operating in very low head sites and also has low installation costs (Elbatran et al., 2015). The geometry for each section of the guiding vane and runner blade was determined by using velocity triangles for the axial-flow cascade, as configured in Figure 2b. However, this study is restricted to numerical optimization and CFD simulation, without making experimental investigations, due to limited research funding.

2.2. Shock-Free Inflow Criterion

This criterion is important to ensure the smoothest entry condition of flow by precisely locating the stagnation point at the end of the camber line of the leading edge, as illustrated in Figure 2a. When the point is located on the upper side of the camber line, the danger of separation increases. On the other hand, if it is located on the lower side of the leading edge camber line,

the diffusion on the surface pressure increases, causing boundary layer transition. Both conditions have a great tendency to increase hydrodynamic losses. Therefore, the ideal condition of the flow entering the cascade is achieved by locating the stagnation point as in the shock-free criterion, so that the pressure distribution across the hydrofoil cascade is smooth and continuous, which can minimize its hydrodynamic losses. Further explanation of the shock-free criterion is given by Lewis (1996).

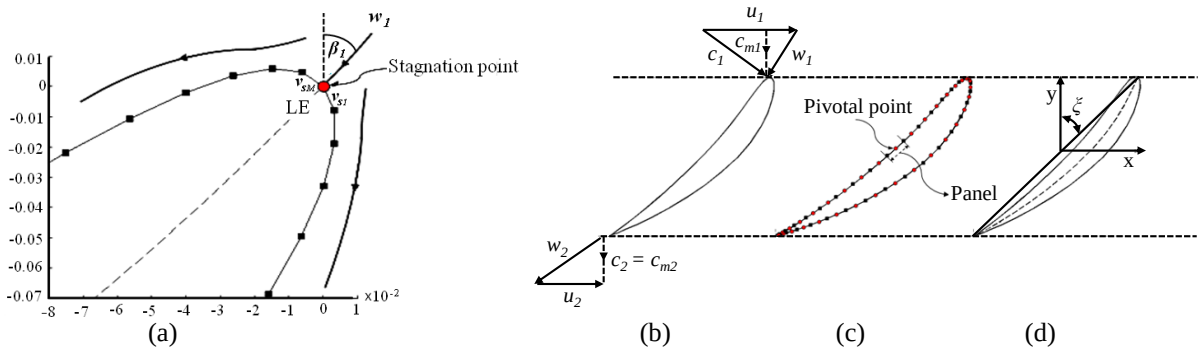

Figure 2 Shock-free inflow condition and surface vorticity panel model in the two-dimensional cascade

The potential flow around the cascade was calculated using the surface vorticity model with a modified coupling coefficient to deal with the turbine cascade. A visualization of this panel in the two-dimensional cascade is shown in Figure 2c; a detailed explanation of this computational scheme was presented by Lewis (1991). Each of the cascade sections from the hub to the tips of guide vane and runner blade has a different tilt angle, called the stagger angle, ξ, as displayed in Figure 2d. The angle is calculated using the velocity triangle of the axial-flow turbine, as shown in Figure 2b. The notations *u*, *c*, *w* and c_m define the tangential, absolute, relative and meridional velocities respectively, while subscripts 1 and 2 denote the inlet and outlet of the cascade.

2.3. Genetic Algorithm

The GA method is among the most popular evolutionary algorithms, mimicking the biological evolution of the natural selection process. Details of the algorithm have been well documented by Yang (2014). The GA flowchart used for the hydrofoil cascade optimization employs the shock-free criterion, as shown in Figure 3.

The hydrofoil cascade optimization of the guide vane comprises two design variables: the stagger angle, ξ, and the maximum camber line of the hydrofoil, M_c. The cost function of this optimization is proposed in Equation 1:

$$\text{minimize } f(\xi, M_C) = \left|\beta_1 - \beta_{1SF}\right| + \left|\beta_2 - \beta_{2SF}\right| \tag{1}$$

where β_1 and β_2 are the inlet and outlet flow angles on the two-dimensional cascade, which are calculated by using the velocity triangle of the axial-flow turbine. Subscript *SF* denotes the shock-free condition.

Meanwhile, there is only one design variable for hydrofoil cascade optimization of the runner blade, namely the stagger angle, ξ. The cost function is proposed in Equation 2:

$$\text{minimize } f(\xi) = \left|\beta_1 - \beta_{1SF}\right| \tag{2}$$

The design space, $\Re^d$, for both optimizations ranges from $-90 \leq \xi \leq 0$ to $0 \leq M_c \leq 14$. For this study, the control parameters of the algorithm are tabulated in Table 1.

Table 1 GA control parameters

Population size	50	
Number of iterations	200	
Parent selection	Crossover operator	Mutation operator
	Tournament	Random
	Guide vane cascade	Runner blade cascade
Crossover probability	0.7	0.8
Mutation probability	0.5	0.5

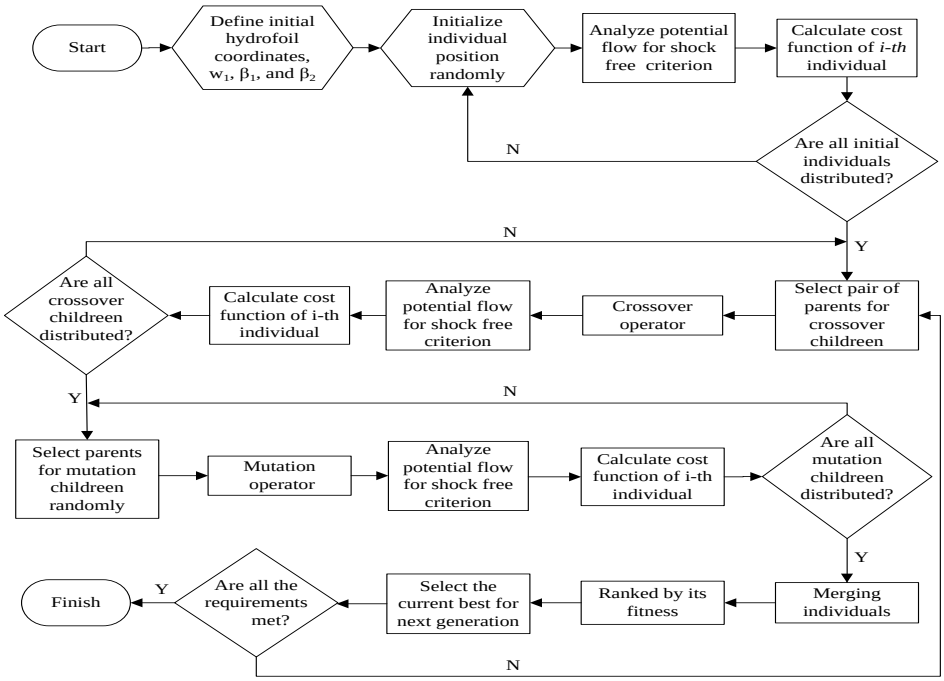

Figure 3 GA flowchart used for two-dimensional cascade optimization using the shock-free criterion

2.4. Numerical Setup

The performance and flow behavior of both turbine designs were predicted using three dimensional steady-state CFD simulation. The computational domain for this study, as shown in Figure 4, was arranged using an axis-symmetric scheme.

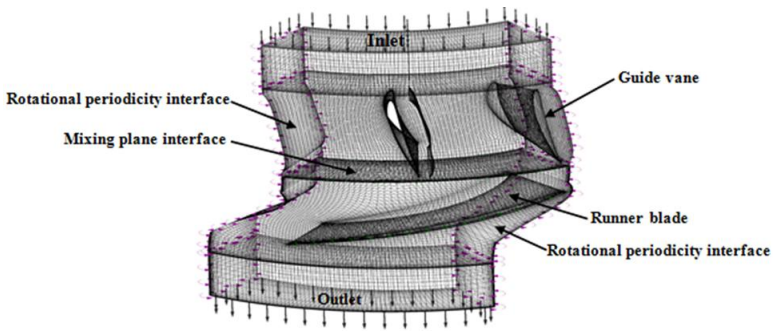

Figure 4 Computational domain of the axial-flow hydraulic turbine

This scheme resulted in simplification of the overall turbine geometry, thus reducing storage costs and saving computational time. The turbulence inside the turbines was predicted using the shear stress transport (SST) *k-ω* turbulence model. The inlet domain was set as total pressure, while the outlet domain was set as static pressure. Both conditions were relative to atmospheric

pressure. Hydraulic turbine efficiency, η_h, was used to predict the performance of both turbine designs by the following equations:

$$\eta_h = \frac{P_{out}}{P_{in}} \times 100\% , \tag{3}$$

$$P_{in} = \rho \times Q_{in} \times g \times h_{tot} . \tag{4}$$

The term P_{out} in Equation 3 is shaft power (W) assuming no mechanical losses; Q_{in} is water discharge at the inlet section (m^3/s), and h_{tot} is total head, which is the head difference between the inlet and outlet sections of the domain.

A grid independent test was conducted to ascertain the independence of the numerical solutions against the grid elements. The test also aimed to establish the most efficient grid size in order to reduce computational costs. The results of the test are plotted in Figure 5.

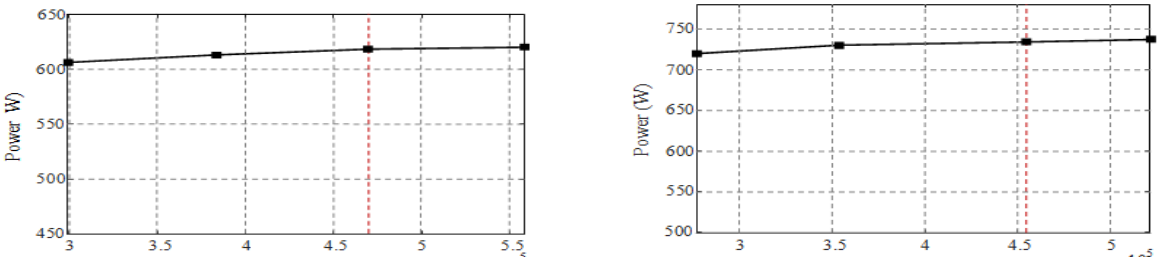

Figure 5 Grid independent results of both turbine designs: (a) initial design; (b) optimized design

The resulting hydraulic power from the four different elements of each turbine design was compared. The first three elements ranged from around 2.9E+05 to 4.7E+05 grid sizes for initial design and around 2.7E+05 up to 4.5E+0.5 grid sizes for optimized design show the same pattern; that is, power tends to increase. Subsequently, the fourth element of around 5.6E+05 grid size for the initial design and 5.2E+06 grid size for the optimized design shows insignificant changes in power compared to the previous grid sizes, which was 0.27% for the initial design and 0.41% for the optimized design. This indicates that further refinement of the elements would not significantly influence the power calculated by the simulation. Hence, for this study the third elements (454572 for the initial design and 469532 for the optimized design), which intersect with red dashed vertical lines in Figure 5, are chosen as the most efficient grid sizes.

3. RESULTS AND DISCUSSION

Value encoding, which decomposes an individual into an array of values, was used for both crossover and mutation operators. Direct value encoding by switching one segment array from pairs of parents to produce crossover children was performed. The results show that this encoding was less effective in reaching an optimal solution whose values are solely in the order of magnitude of E-3. The small number of design variables meant that this switching method only had a small combination of values in the search space, which resulted in non-optimal solutions. To achieve more diversity in the solution space, modification was made to the encoding in the randomly distributed search space, with a specified genes array threshold, α,

ranging from $-\gamma \leq \alpha \leq (1+\gamma)$. By applying gamma, γ, which is an extra range factor for direct value encoding, the new switching method for the crossover operator is shown in Equation 5:

$$\begin{aligned}&\textbf{function } [\xi c, M_{c,c}] = \text{crossover } (\xi p, M_{c,p}, \gamma, \text{lbs}, \text{ubs}, \text{lbc}, \text{ubc})\\ &\alpha = \text{unifrnd } (-\gamma, 1+\gamma, \text{size } (\xi p));\\ &\xi c = \alpha.* \xi p + (1- \alpha).* M_{c,p};\\ &M_{c,c} = \alpha.* M_{c,p} + (1- \alpha).* \xi p;\\ &\textbf{end}\end{aligned} \quad (5)$$

in which a γ of 0.8 was chosen for this study. ξ is the stagger angle and M_c is the maximum camber line of the hydrofoil. It is important to ensure that $lbs \leq \xi_c \leq ubs$ and $lbc \leq M_c \leq ubc$. *lbs* and *ubs* are the lower and upper bounds of the stagger angle, and that *lbc* and *ubc* are the lower and upper bounds of the maximum camber line. Subscripts *c* and *p* denote child and parent respectively. Finally, comparative results of both switching methods for the crossover operator are shown in Figure 6.

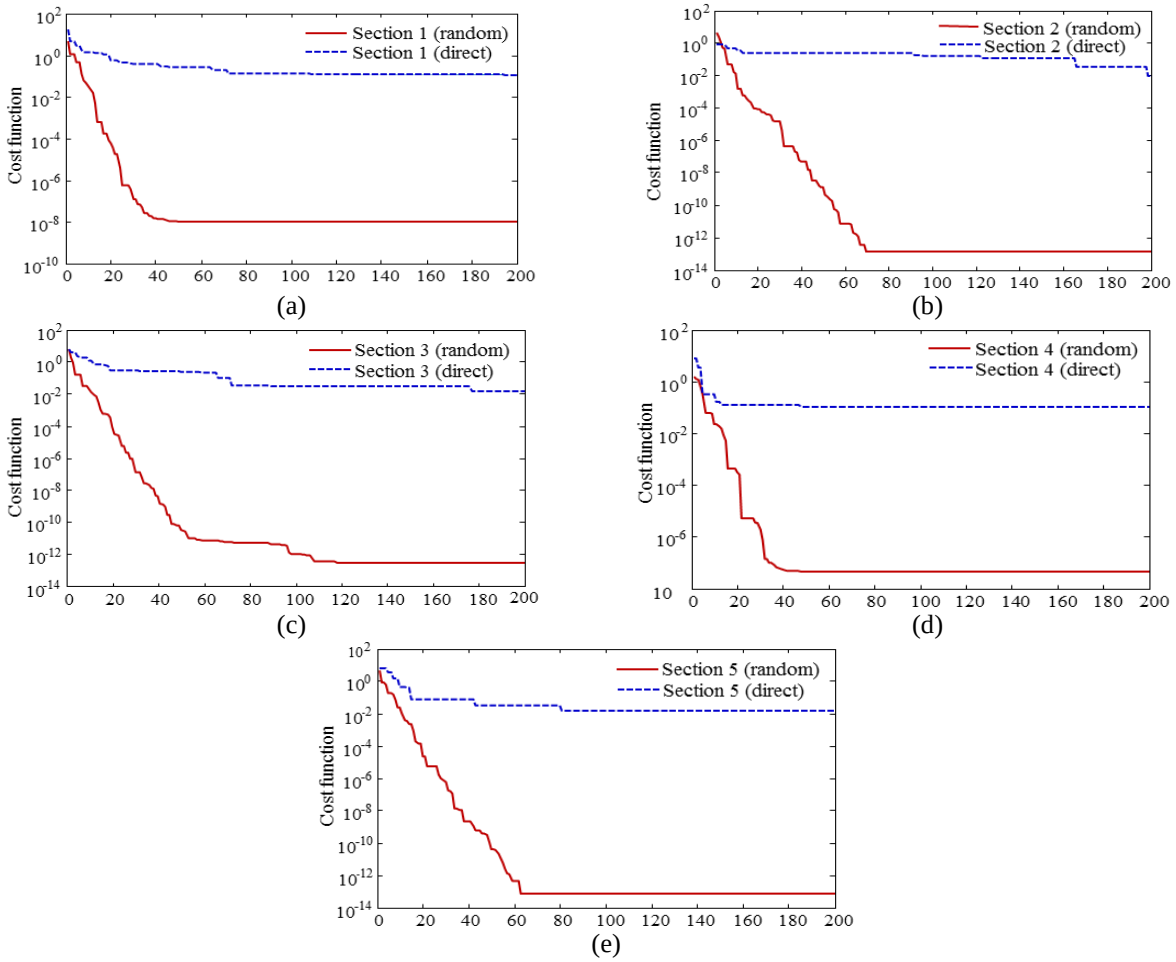

Figure 6 Performance comparison between the direct and random switching methods for the crossover operator in each guide vane cascade section

In this study, the search process performed by the algorithm to find the optimal value of each design variable was evaluated within 200 iterations in one cycle optimization. The results show that the random distribution switching method for the crossover operator outperformed the direct switching method on each cascade section. This is mainly because gamma, γ, made the search space from the genes of the parents more varied, resulting in more diverse solutions in each generation and giving the high possibility of finding a high quality solution, as measured

by its cost function. Detailed values of the cost functions and design variables in each section of the guide vane cascade using random distribution are shown in Table 2.

Table 2 Optimal design variable values for the guide vane cascades and their cost functions

Section	Guide vane cascades		
	Stagger angle, ξ	Maximum camber line, M_c	Cost function, f(x)
1	-13.76	8.89	1.45E-10
2	-12.61	8.00	1.22E-13
3	-11.64	7.26	4.15E-14
4	-10.81	6.62	9.13E-14
5	-10.08	6.07	1.23E-13

A global solution for each cascade section which is less than E-9 means that the method has successfully improved the performance of the direct switching method. Meanwhile, the performance of the GA in optimizing the stagger angle in each section of the runner blade cascades is shown in Figure 7a.

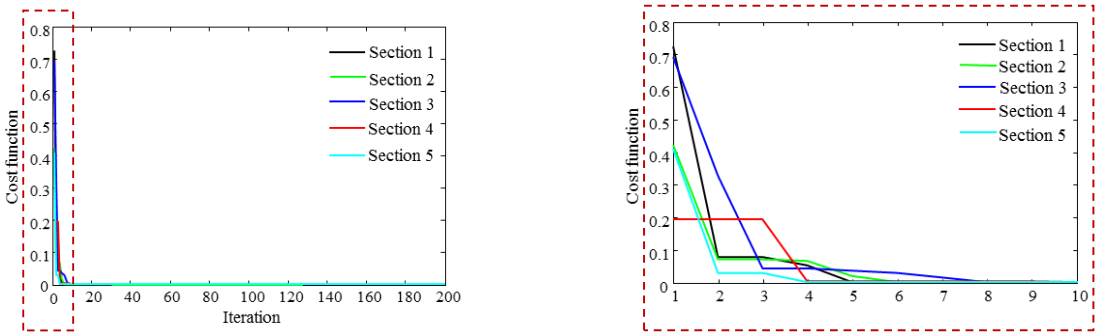

Figure 7 Cost function evolution of each section of the runner blade cascades

Figure 7b gives a detailed view of the first ten iterations of the cost function evolution. The algorithm converged shortly after 30 iterations in each section of the runner blade cascades by using random distribution crossover. The order of magnitude of the average cost function is E-14. Detailed values are listed in Table 3.

Table 3 Optimal design variable and its cost function in each section of the runner blade cascades

Section	Runner blade cascades	
	Stagger angle, ξ	Cost function, f(x)
1	-65.65	1.42E-14
2	-68.38	0.00E+00
3	-70.48	2.84E-14
4	-72.17	1.42E-14
5	-73.59	2.84E-14

As shown in Table 4, the algorithm also has the ability to find the global optimum solution in section two of the runner blade cascade, which means that the difference between the inlet flow angle resulting from optimizing the design variable of the stagger angle and the related shock-free angle for a given flow condition is zero. Therefore, it can be concluded that the GA

algorithm with a random distribution crossover is an efficient optimization algorithm to find the optimal design variables for both guide vane and runner blade cascades.

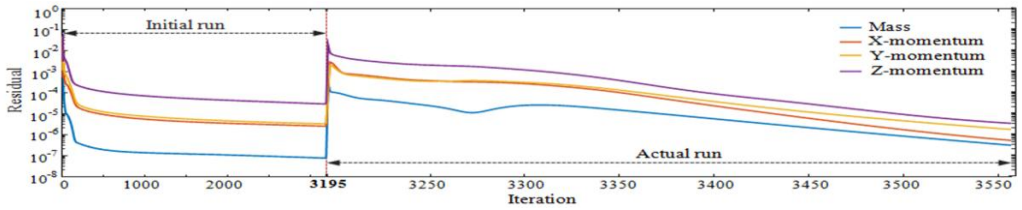

Figure 8 Convergence history during the iteration of the conservation equations

After cascade optimization of the initial turbine design had been processed, the numerical simulation using the CFD approach was conducted to predict the performance of both turbine trials. The convergence history during the iteration of the conservation equations, which was solved by the commercial CFD solver ANSYS CFX, is plotted in Figure 8. Each simulation run is divided into two sequential phases, i.e. the initial run and actual run. The numerical results from the initial run are used as the initial condition for the actual simulation run. To reach convergence, the residual target of 1.0E-04 for all the governing equations must be achieved. These criteria are met for about 3200 iterations in the initial run and 350 iterations in the actual run. The initial run, as shown in Figure 8, takes much more computational time to reach convergence because there are several numerical assumptions regarding the physical flow condition based on the design condition. A comparison of the velocity contour between both turbine designs at the meridional plane is shown in Figure 9.

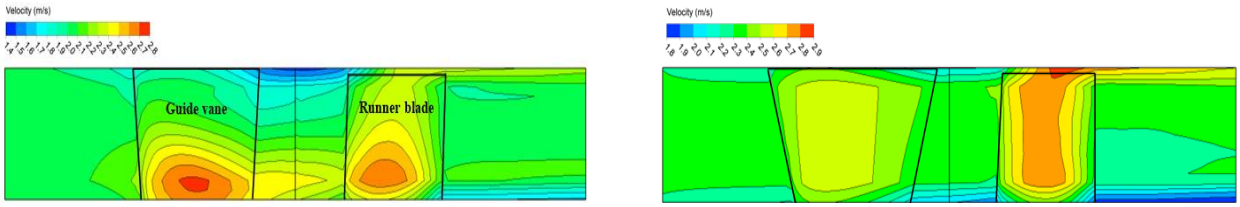

(a) (b)

Figure 9 Velocity contour of turbine passages at the meridional plane: (a) initial design; (b) optimal design

Referring to the velocity contour of the initial design at the meridional plane, a gradual decrease in velocity is observed near the hub region of both guide vanes and runner blade passages. The velocity degradation spreads in oval patterns towards the surrounding areas and is centered around approximately 0.15 and 0.2 spanwise locations of the guide vanes and runner blade respectively. For the optimal design, the velocity pattern is slightly different from the previous one, although it shows the same occurrence of velocity degradation. The trapezoid patterns of velocity deflation, which are centered around 0.5 spanwise locations, are observed in both the guide vane and runner blade areas. In comparison with the initial design, the velocity of the optimized design is more stable along the spanwise and streamwise directions, meaning that the changes in velocity do not occur intensively in both directions, as was the case with the initial design. The tip clearance velocity of the optimized design, which is located in the space between the tip of the runner blade and the turbine shroud, is higher than that of the initial design. Moreover, the optimized design tip clearance is observed to have the highest velocity in the passages. However, it was found that the tip leakage velocity of both designs displays the same behavior; that is, the velocity tends to accelerate when entering these locations. This occurence was the root cause of the tip leakage loss, which was the power loss due to leakage in the flow rate.

The simulation results for the pressure contour of both turbine designs are shown in Figure 10.

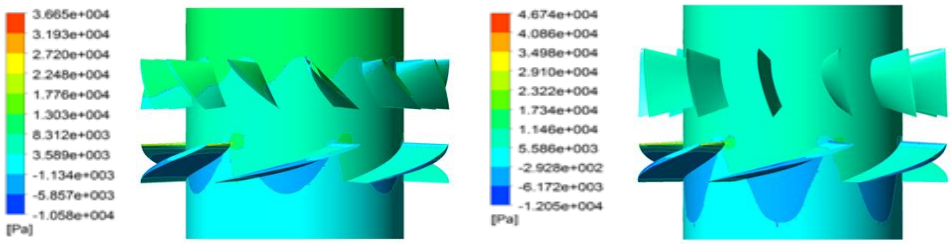

(a) (b)

Figure 10 Pressure contour of the initial and optimized turbine designs

The pressure contour of the optimized turbine design, as shown in Figure 10b, displays no significant pressure degradation on the pressure side of the guide vanes, as is the case in Figure 10a, which is the pressure contour of the initial turbine design. This allows hydraulic energy transfer from the inlet section to flow smoothly through the guide vane without losing significant pressure, so the potential energy of the water can be utilized optimally by the runner blades. A detailed blade-to-blade view of the pressure contour of both turbine designs is compared in Figure 11.

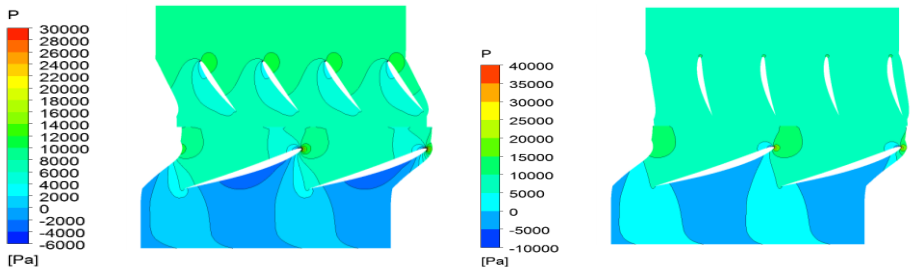

(a) (b)

Figure 11 Blade-to-blade view of pressure contour in 0.5 spanwise location: (a) initial design; (b) optimal design

Comparison of the pressure in the 0.5 spanwise location between both turbine designs shows the same pattern observed in the hub region. The pressure contour of the initial design decreases on the pressure side near the trailing edge region and below the suction side of the guide vanes. Conversely, this sudden pressure deflation does not occur in the guide vane passage of the optimized design. This is mainly because the angle of inclination with respect to the vertical axis of the optimized guide vanes is less steep than the initial one, so there is no significant blockage of flowing water from the inlet which could cause pressure degradation. Furthermore, the pressure pattern in the runner blade passage for both turbine designs is very similar. The pressure at the front of the runner's leading edge is the highest compared to other areas in the passages. This is mainly because the leading edge is the main area of the blade which directly withstands the resistance of the flowing water when the runner rotates. It is observed that the area below the suction side of the runner for both designs has negative pressure. This condition has a great tendency to cause cavitation. Therefore, a material with high resistance to corrosion needs to be considered as the main one for the runner blades in order to minimize replacement costs.

Further analysis regarding pressure distribution in both runner designs, and blade loading comparison between the initial and optimized designs in different span locations, is shown in Figure 12.

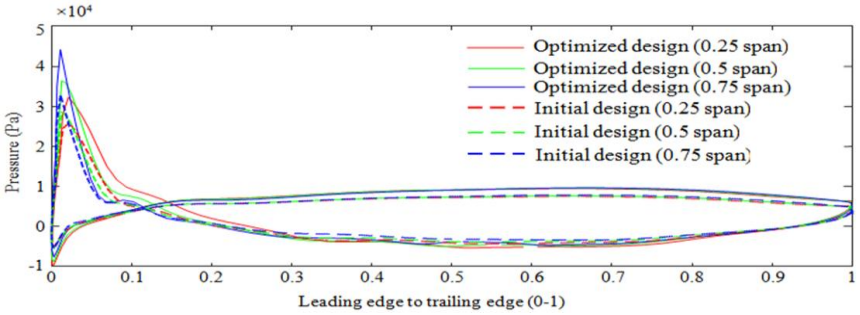

Figure 12 Blade loading comparison between initial and optimized designs in different span locations

A sudden increase in blade pressure around the leading edge of the pressure side is found in different span locations for both turbine designs. Despite the increase in pressure fluctuation along with the higher span location, the optimized runner has higher pressure fluctuation compared to the initial runner at the corresponding span location. Subsequently, pressure falls sharply until about 0.1 chord length and then slowly decreases to around the middle of the chord length. Meanwhile, the pressure distribution on the suction side of both runner designs decreases over a short distance, before increasing rapidly to about 0.02 chord length. Contrary to the fluctuation on the runner's pressure side, the blade loading around the leading edge of the suction side is higher than that of the pressure side, although the pressure difference of both runner designs at the corresponding span location is insignificant. As shown in Figure 12, the optimized design symbolized by solid lines has a higher pressure difference along the runner surface compared to the initial design, causing more pressure when producing torque. The performance of both turbine designs is evaluated by their hydraulic efficiency, as plotted in Figure 13.

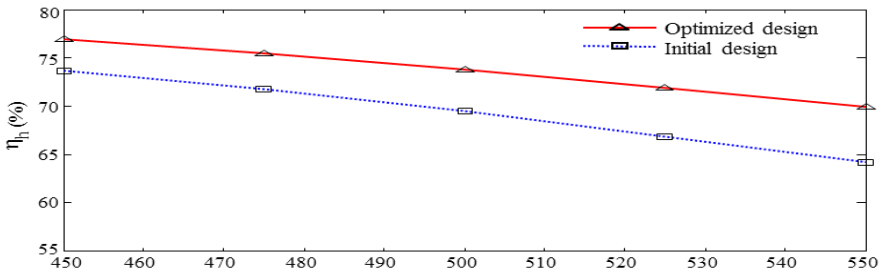

Figure 13 Performance comparison between initial and optimized turbine designs under various operating conditions

The plot shows a performance comparison between both turbine designs under various operating conditions. From the viewpoint of fluid dynamics analysis, hydraulic efficiency, η_h, is the main parameter for quantitatively evaluating the performance of the hydraulic turbine at an early design stage. Because the simulation was only performed in limited operating conditions, the performance characteristics of the turbine cannot be completely evaluated. However, the hydraulic performance, as shown in Figure 13, which includes performance in nominal operating conditions, is adequate for evaluating the nominal performance of both designs. Based on the simulation results, the performance of the optimized turbine design resulted in 73.72% greater hydraulic efficiency in nominal operating conditions, which means it is 4.29% higher than the performance of the initial turbine design. Furthermore, the optimized turbine design also outperforms the initial one in several operating conditions, ranging from 450 to 550 rpm.

4. CONCLUSION

Numerical optimization of an axial flow hydraulic turbine using two-dimensional cascade analysis has been performed. The GA was found to be an efficient optimizer to satisfy the shock-free criterion in the two-dimensional hydrofoil cascade for the axial-flow hydraulic turbine. However, the switching method used for the crossover operator of the algorithm should be carefully noted. From the optimization results, the crossover operator with the random distribution switching method resulted in more robust solutions compared to the direct method because of its diversity. By applying this method, the cost function value in each guide vane cascade section is less than E-09, while the runner blade has an average value of E-14. Furthermore, the performance of both turbine designs was predicted using the three-dimensional CFD approach. The simulation results show that the optimized turbine design improves the hydraulic performance of the initial turbine design by 4.29% under nominal operating conditions. Moreover, the hydraulic performance of the optimized turbine design also outperforms the performance of the initial turbine design under various operating conditions, ranging from 450 to 550 rpm. Therefore, it can be concluded that the GA as an optimizer used to achieve the shock-free criterion in two-dimensional cascades has successfully improved the hydraulic performance of the initial turbine design.

5. ACKNOWLEDGMENT

The Authors would like to thank to Research Centre for Electrical Power and Mechatronics – Indonesian Institute of Sciences (P2 Telimek – LIPI) for supporting this project.

6. REFERENCES

Bostan, I., Gheorghe, A.V., Dulgheru, V., Sobor, I., Bostan, V., Sochirean, A.I., Bostan, A.V., Gheorghe, V., Dulgheru, I., Sobor, V., Bostan, A., Sochirean, 2013. *Chapter 4 – Kinetical Energy of River Running Water. Resilient Energy Systems: Renewables: Wind, Solar, Hydro*, Springer, p. 202

Da Cruz, A.G.B., Mesquita, A.L.A., Blanco, C.J.C., 2008. Minimum Pressure Coefficient Criterion Applied in Axial-Flow Hydraulic Turbines. *Journal of the Brazilian Society of Mechanical Sciences*, Volume 30(1), pp. 30–38

Drtina, P., Sallaberger, M., 1999. Hydraulic Turbines – Basic Principles and State-of-the-art Computational Fluid Dynamics Applications. *In*: Proceedings of the Institution of Mechanical Engineers Part C Journal of Mechanical Engineering Science, Volume 213(1), pp. 85–102

Elbatran, A.H., Yakoob, O.B., Ahmed, Y.M., Shabara, H.M., 2015. Operation, Performance and Economic Analysis of Low Head Micro-hydropower Turbines for Rural and Remote Areas : A Review. *Renewable and Sustainable Energy Reviews*, Volume 43, pp. 40–50

International Electrotechnical Commission 60193 standard, 1999. *IEC 60193 standard: Hydraulic Turbines, Storage Pumps and Pump-turbines – Model Acceptance Test*. International Electrotechnical Commission, p. 55

Jacobs, E., Ward, K., Pinkerton, R., 1933. *The Characteristics of 78 Related Airfoil Sections from Tests in the Variable-density Wind Tunnel*. NACA Report 460

Kim, J.-H., Cho, B.-M., Kim, S., Kim, J.-W., Suh, J.-W., Choi, Y.-S., Kanemoto, T., Kim, J.-H., 2017. Design Technique to Improve the Energy Efficiency of a Counter-rotating Type Pump-turbine. *Renewable Energy*, Volume 101, pp. 647–659

Kinsey, T., Dumas, G., 2017. Impact of Channel Blockage on the Performance of Axial and Cross-flow Hydrokinetic Turbines. *Renewable Energy*, Volume 103, pp. 239–254

Lewis, R.I., 1991. *Vortex Element Methods for Fluid Dynamic Analysis of Engineering Systems*, Cambridge Univeristy Press, New York, USA

Lewis, R.I., 1996. *Turbomachinery Performance Analysis*, Elsevier Science & Technology Books, London, UK

Muis, A., Sutikno, P., Soewono, A., Hartono, F., 2015. Design Optimization of Axial Hydraulic Turbine for Very Low Head Application. *Energy Procedia*, Volume 68, pp. 263–273

Muis, A., Sutikno, P., Soewono, A., Hartono, F., 2016. Optimal Design of Two-Dimensional Cascade with Shock- Free Inflow Criterion. *International Journal of Fluid Machinery and Systems*, Volume 9(4), pp. 362–369

Prasad, V., 2012. Numerical Simulation for Flow Characteristics of Axial Flow Hydraulic Turbine Runner. *Energy Procedia*, Volume 14, pp. 2060–2065

Ramos, H.M., Simão, M., Borga, A., 2013. Experiments and CFD Analyses for a New Reaction Microhydro Propeller with Five Blades. *Journal of Energy Engineering*, Volume 139(2), pp. 109–117

Riglin, J., Carter, F., Oblas, N., Schleicher, W.C., Daskiran, C., Oztekin, A., 2016. Experimental and Numerical Characterization of a Full-scale Portable Hydrokinetic Turbine Prototype for River Applications. *Renewable Energy*, Volume 99, pp. 772–783

Schleicher, W.C., Riglin, J.D., Oztekin, A., 2015. Numerical Characterization of a Preliminary Portable Micro-hydrokinetic Turbine Rotor Design. *Renewable Energy*, Volume 76, pp. 234–241

Sutikno, P., Adam, I.K., 2011. Design, Simulation and Experimental of the Very Low Head Turbine with Minimum Pressure and Free Vortex Criterions. *International Journal of Mechanical and Mechatronics Engineering*, Volume 11(1), pp. 9–15

Yang, X.-S., 2014. *Chapter 5 - Genetic Algorithms, In Nature-Inspired Optimization Algorithms*. Elsevier, Oxford, p. 78